VNU Journal of Science: Mathematics – Physics, Vol. 42, No. 2 (2026) 41-54

VNU Journal of Science: Mathematics - Physics

Journal homepage: https://js.vnu.edu.vn/MaP

Original Article

# The Density-Structure Correlations in $Al_2O_3$Glasses: Insights from Molecular Dynamics Simulation

Nguyen Thi Thanh Ha*

*School of Engineering Physics, Hanoi University of Science and Technology,*
*1 Dai Co Viet, Hai Ba Trung, Hanoi, Vietnam*

Received 30th September 2025
Revised 29th November 2025; Accepted 28th April 2026

**Abstract:** The relationship between structure and density in $Al_2O_3$ glass has been studied by mean of molecular dynamic simulation. Simulation results reveal that the structure of $Al_2O_3$ is formed by $AlO_x$ structural unit. Under densification, there is the transformation from tetrahedral to octahedral structure. The $AlO_x$ structural units tend to form the cluster of $AlO_x$ units. Alumina exhibits polymorphism and heterogeneous structure due to the presence of $AlO_x$ clusters and two-domain types (D4–D5 or D5–D6) in the intermediate density range. Moreover, a continuous random network of basic structural units linking to each other via with corner-sharing, edge-sharing, face-sharing bond. At low density region, the basic structural units are mainly linked via bridge oxygen and the connectivity between $AlO_x$ is mainly corner sharing bonds. The numbers of corner-sharing and edge-sharing bonds vary in opposite directions. The basic structural units are barely bonded to each other via face-sharing bond. In the model, there is the existence of the free volume region. The distribution of free volumes depends on density. It has the Gaussian form and the position of the peak tends to shift to the left under compression. As densnit increases, the void radius decreases rapidly.

*Keyword:* Molecular dynamic, structural transformation, structural heterogeneity, polymorphism, density.

## 1. Introduction

Oxide glasses are important materials and have been widely used in optical, biological, microelectronics and high technology materials. Therefore, the oxide glasses have been the subject of many experimental and simulation studiess [1-5]. In which, the effect of compression on structure and dynamical properties of oxide glasses is an issue that has been researched diligently. Structural

* Corresponding author.
*E-mail address:* ha.nguyenthithanh1@hust.edu.vn

https//doi.org/10.25073/2588-1124/vnumap.5081

transformations have been observed using X-ray Raman scattering, infrared spectroscopy, and X-ray diffraction. Their structures consist of a random network of corner-sharing tetrahedra [6,7]. Polymorphism and heterogeneous structure occurs when tetrahedral units transform gradually into higher co-ordinated octahedral units [7-10] under densification.

In addition, alumina is widely used in various engineering fields because it possesses special properties, including wear resistance, low electrical conductivity, and high thermal and chemical stability [11-13]. The local microstructure of $Al_2O_3$ has been investigated via many method. Using interpretations of NMR [14], XANES [15], x-ray, NMR [16, 17] and neutron diffraction [18], the results have suggested that alumina comprises of a mixture of 4- and 6-fold coordinated Al. And lumina is supposed to comprise of a quasi-diphasic structure composed of dense corundum clusters and a less dense $AlO_4$ structure surrounded by octahedral vacancies. Hence, the model exhibits a heterogeneous structural [15]. Moreover, the experimental results confirm the formation of $OAl_3$ triclusters associated with the large contribution of edge-sharing Al–O polyhedral. The formation of edge-sharing $AlO_5$ and $AlO_6$ polyhedral is not the same as the corner-sharing tetrahedra motif of Zachariasen's conventional glass formation concept [19]. Much useful information about microstructure of alumina can be provided by computer simulation [20-22]. Molecular dynamics simulations are employed to study the structure of $Al_2O_3$. The simulation results revealed that liquid alumina consists of predominantly 5-fold coordination, with appreciable 4- and 6-fold polyhedral present [20]. Using both X-ray and neutron diffraction combined with molecular dynamics (MD) simulations, Skinner et al indicated alumina contains mostly $AlO_4$, but with a significant fraction of $AlO_5$ units, and only minor fractions of $AlO_3$ and $AlO_6$ [23]. The structural transformation from a tetrahedral to an octahedral network in alumina was found to occur at a density range of 3.6 - 4.5 g c/$m^3$ [24, 25]. However, the atomistic mechanism and the factor affect to the process of structural transformation in glass material have not been successfully identified. Therefore, in this study we used structural unit, domain definitions, different types of bridge-oxygen connectivity as well as free volume regions (voids, vacancies) to clarify the influence of density on the structural transformation and structural heterogeneity in $Al_2O_3$ glass.

## 2. Computational Procedure

MD simulation is carried out for a model consisted of 2200 Al and 3300 O at a temperature of 600 K and the range of density from 2.83 to 4.81 g/$cm^3$. The Born–Mayer type pair potential is used to contruct the simulation model [26]. All atoms move by applying the Verlet algorithm at the time step of about 1.0 fs. The first, starting of the simulation, a sample is obtained by randomly placing all atoms in a simulation box and then relaxing at 5000 K. Then, the sample is cooled down to 3500 K and relaxed at this temperature for 2-3 ns. This model is denote M1. Next, we compress model M1 to densities different to produce 10 models $Al_2O_3$ glass at temperature of 3500 K and density in the from 2.83 to 4.81 g/$cm^3$ range. These models has been relaxed for a long relaxation ($10^7$ MD time steps). A long relaxation has been done to get equilibrium state using isothermal-isobaric (NPT) ensemble (Here N, P and T are constants, with N, P and T the number of atoms, pressure and temperature, respectively). After that, the models are cooled to 600 K with cooling rate of 2.5 K/ps. Next, these models with different densities are relaxed for $10^6$ MD time steps. In order to improve statistics, all quantities of considered structural data are determined by averaging over the 1000 configurations during the last simulation ($10^5$ MD steps).

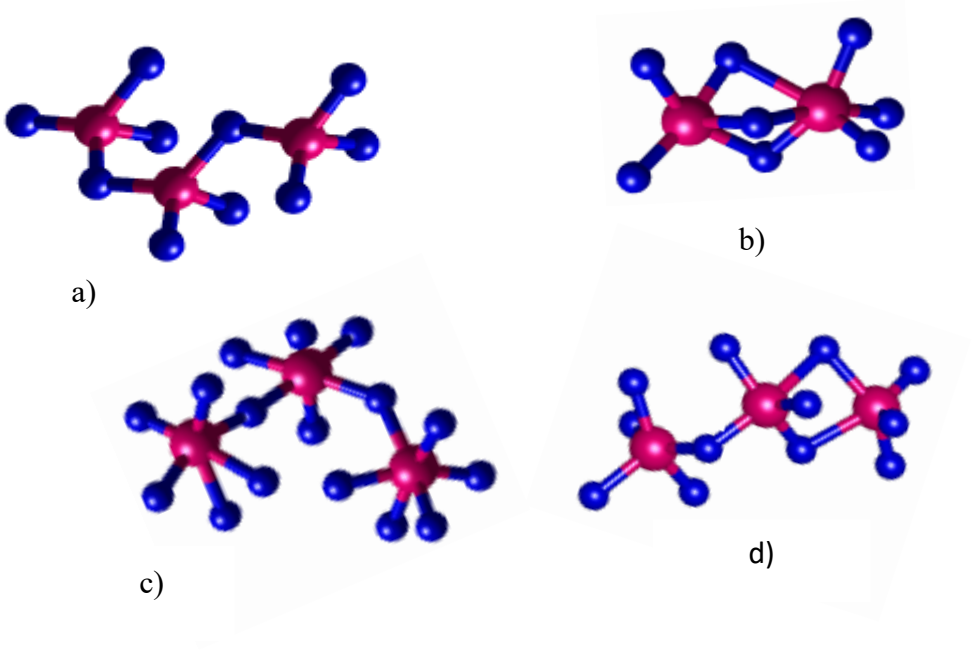


Figure 1. Schematic illustration the cluster, domain Dx (a,b,c) and the corner- sharing bonds (a), edge-sharing bond (d), face- sharing (b) in $Al_2O_3$ glass.

To determine the relationship between the concentration of structural units and the density, we employed multiple linear regression. The equation representing this relationship is as follows:

$$\rho = F + a^* C_{AlO4} + b^* C_{AlO5} + c^* C_{AlO6} \quad (2.\ 1)$$

Where $\rho$ (g/cm$^3$) is density; *a, b, c, d, F* are constants that are calculated by fitting the simulation data of density to Eq. (1); and $C_{AlO4}$, $C_{AlO5}$, $C_{AlO6}$ are the fraction (%) of $AlO_x$ (x=4,5,6). We use the cutoff distances $r_{cutoff}$ which are chosen from the first minimum of pair radial distribution function to calculate the fraction (%) of $AlO_x$ unit. $r_{cutoff}$ is equal to 2.55 Å for Al-O pair. In this study, we employ following the notations and definitions. The $AlO_x$ cluster comprises a subset of atoms that belong to the same structural unit $AlO_x$ (x=4,5,6). Meanwhile Dx domain comprises $O_{xx}$ (Oxygen atom bonds with aluminum atoms having the same coordination numbers) and Al atoms having the same coordination numbers. The Fig. 1 describes the cluster and domain Dx in $Al_2O_3$. In which, domain D4, D5, D6 all have 5 atoms and remaining oxygen atoms is domain boundary (DB). Meanwhile, the $AlO_4$ cluster has 13 atoms (see Fig. 1a), the $AlO_5$ cluster has 9 atoms (see Fig. 1b) and the $AlO_6$ cluster has 16 atoms (see Fig. 1c). The $AlO_x$ basic structural units link to each other via one, two and three bridging oxygens (BOs). They are called corner-sharing, edge-sharing, face-sharing bond, respectively. The Fig. 1a, c discribe corner-sharing bond in cluster $AlO_4$ and $AlO_6$, Fig 1b displays edge-sharing bond in cluster $AlO_5$ and Fig. 1d displays edge-sharing bond in cluster $AlO_5$.

## 3. Results and Discussion

We evaluated the relationship between structure and density in glass materials via the configurations of $Al_2O_3$ with different density. Firstly, the reliability of models is determined via the PRDF $g_{ij}(r)$ for all three pairs. The distance of the first peak, the fractions of coordination numbers are compared with the

results of simulations [27, 28] and experimental data [18]. Our simulated results are also good in agreement with reference. The detailed characteristics of the PRDF $g_{ij}(r)$ under densification are summarized in Table 1 and Fig. 2.

Table 1. Structural characteristics of $Al_2O_3$ glass; $r_{ij}$, $g_{ij}$ – the position and height of first peak in *PRDF*; $C_{AlO4}$, $C_{AlO5}$, $C_{AlO6}$, $C_{AlOother}$ and $C_{OAl3}$, $C_{OAl4}$, $C_{OAlother}$ are the fraction (%) of $AlO_x$ *(x=4,5,6, other)* and $OAl_y$ *(y=3,4, other)* units, respectively

| Model<br>$\rho$ (g/cm$^3$) | M1<br>2.83 | M2<br>3.65 | M3<br>3.71 | M4<br>3.85 | M5<br>3.92 | M6<br>4.05 | M7<br>4.17 | M8<br>4.34 | M9<br>4.66 | M10<br>4.81 | MD<br>3.0<br>[27] | Exp<br>-<br>[18] |
|---|---|---|---|---|---|---|---|---|---|---|---|---|
| $r_{Al-Al}$, [Å] | 3.14 | 3.06 | 3.06 | 3.10 | 3.08 | 3.08 | 2.98 | 2.96 | 2.86 | 2.86 | 3.22 | 3.20±0.55 |
| $r_{Al-O}$, [Å] | 1.72 | 1.70 | 1.70 | 1.70 | 1.70 | 1.70 | 1.72 | 1.70 | 1.74 | 1.74 | 1.78 | 1.80±0.21 |
| $r_{O-O}$, [Å] | 2.78 | 2.66 | 2.54 | 2.60 | 2.56 | 2.58 | 2.46 | 2.44 | 2.46 | 2.44 | 2.81 | 2.80±0.58 |
| $g_{Al-Al}$ | 3.78 | 4.67 | 4.90 | 4.77 | 4.75 | 4.63 | 4.17 | 4.58 | 3.74 | 3.69 | - | - |
| $g_{Al-O}$ | 8.35 | 5.83 | 5.70 | 5.71 | 5.69 | 5.54 | 5.14 | 5.69 | 6.03 | 6.07 | - | - |
| $g_{O-O}$ | 2.95 | 3.84 | 3.85 | 3.75 | 3.65 | 3.55 | 3.57 | 3.64 | 4.27 | 4.09 | - | - |
| $C_{AlO}$ | 74.82 | 31.32 | 16.55 | 25.59 | 18.36 | 12.18 | 7.82 | 3.82 | 2.09 | 0.95 | 85.0 | 56.0 |
| $C_{AlO5}$ | 24.00 | 48.68 | 49.45 | 50.91 | 51.32 | 48.18 | 36.41 | 34.09 | 26.00 | 19.82 | 13.0 | 22.0 |
| $C_{AlO6}$ | 0.86 | 19.91 | 33.73 | 23.45 | 30.05 | 38.82 | 54.82 | 58.32 | 66.18 | 70.86 | 6.0 | - |
| $C_{AlOother}$ | 0.32 | 0.09 | 0.27 | 0.05 | 0.27 | 0.82 | 0.95 | 3.77 | 5.73 | 8.36 | - | - |
| $C_{OAl}$ | 78.15 | 27.37 | 18.57 | 22.91 | 19.03 | 14.34 | 9.26 | 7.22 | 3.92 | 3.37 | 74.0 | - |
| $C_{OAl4}$ | 3.50 | 71.35 | 78.93 | 75.25 | 78.93 | 83.17 | 85.78 | 89.19 | 65.49 | 63.46 | 1.0 | - |
| $C_{OAlother}$ | 18.35 | 1.28 | 2.50 | 1.83 | 2.04 | 2.49 | 4.95 | 3.59 | 26.48 | 27.88 | - | - |

It can be that the Al–O bond distance is almost independent of density. It has value about 1.70±0.02Å. Meanwhile the Al-Al and O-O bond distances are significantly dependent on density. As the density increases from 2.83 to 4.81 g/cm$^3$, the Al-Al and O-O bond distances decrease. Moreover, the height of first peak of radial distribution function for the pair Al-O decreases and mean coordination numbers for all pairs of atoms increase under compression. The simulation showed that the size of structural units as well as the length of connectivity between them also decrease when density increases. According the chosen densities, the glass $Al_2O_3$ model has the tetrahedral network structure at the density of 2.83 g/ cm$^3$.The fraction of $AlO_4$ accounts for 74.82%. In model M2, the fraction of $AlO_4$ and $AlO_5$ is equal to 31.32% and 48.68%, respectively. In model M7, the fraction of $AlO_5$ and $AlO_6$ is equal to 36.41% and 54.82%, respectively. For the model M10, the structure unit $AlO_x$ is mainly $AlO_6$ (70.86%) (see Table 1). It means that structure of glass is a closed packed-like structure at high density. Furthermore, the density of the simulated model can be determined based on the concentrations of structural units according to equation (2.1) as follows:

$$\rho = 3.580006 + 0.012398 * C_{AlO4} - 1.225352 * C_{AlO5} + 0.577901 * C_{AlO6} \quad (2.1)$$

The density of alumina fitted by equation (2.1) is consistent with the simulation results, as illustrated in Fig 3. At ambient pressure, the density of the system is 2.83 g/cm³, and it increases to 4.81 g/cm³ at a pressure of 100 GPa. The density of amorphous alumina increases significantly in the pressure range of 0- 40 GPa. It means that glass alumina undergoes a structural phase transition under compression. At low density, the system is primarily composed of tetrahedral structures, while at high pressure it adopts

octahedral structures. Upon compression, the system transforms from the low-density phase to the high-density phase.

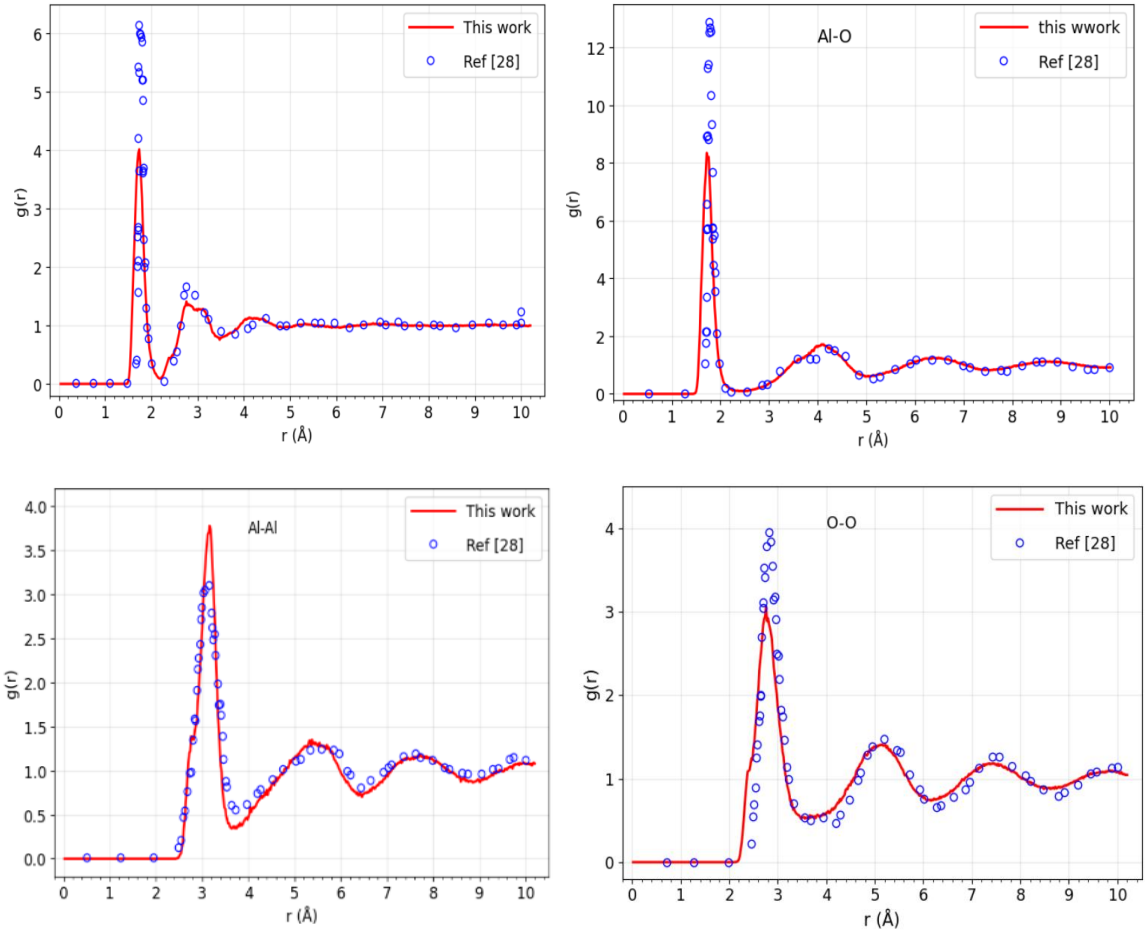


Figure 2. MD results for the total and partial pair distribution functions of amorphous alumina at 600 K and ρ = 2.83 g/cm³, compared with the model at 300 K and ρ = 2.81 g/cm³ (Ref. [28]).

The Fig. 4 presents the dependence of the fractions of $AlO_x$ unit on density in $Al_2O_3$ glass. The results show that the structure of $Al_2O_3$ depend on the density. There is the transformation from tetrahedral ($AlO_4$) to octahedral ($AlO_6$) structure under densification. Namely, the fraction of $AlO_4$ monotonously decreases while fraction of $AlO_6$ increases with increasing density. The fraction of $AlO_5$ increases and has a maximum near the point of 3.92 g/cm$^3$ density. Therefore, at the low density (2.83 g/cm$^3$) and high density (4.81 g/cm$^3$), the $Al_2O_3$ structure consists of the main $AlO_4$ and $AlO_6$- phase, respectively. Meanwhile the structure of $Al_2O_3$ consists of two main phases ($AlO_4$, $AlO_5$) and ($AlO_5$, $AlO_6$) at 3.65 g/cm$^3$ and 4.17 g/cm$^3$ density, respectively. It means that the $Al_2O_3$ structure exists only one phase at low or high density and two phases at intermediate density region. The $AlO_4$ unit is stable at low density and the $AlO_5$ and $AlO_6$ units are stable at high density. Under densification, there is a continuous transition from $AlO_4$ units to $AlO_5$ units, and finally to $AlO_6$ units as density increases [13, 15, 16, 18, 23].

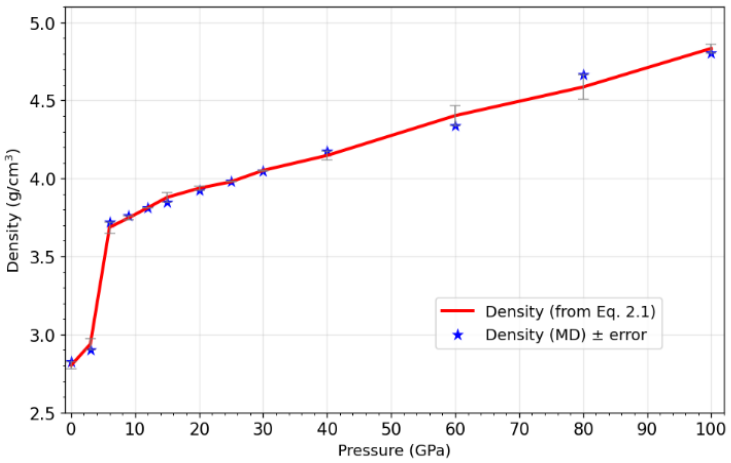


Figure 3. The density of $Al_2O_3$ model at different pressures

Considering the distribution of structural units $OAl_y$ (*y=3,4, other*), the fraction of $OAl_3$ units is equal to 78.15% at 2.83 g/cm$^3$ density. It decreases meanwhile fraction of $OAl_4$ unit increases under densification. Thus, average coordination number of oxygen tends to increase from three-fold (at ambient pressure) to four-fold (at high pressure) (see Fig. 5).

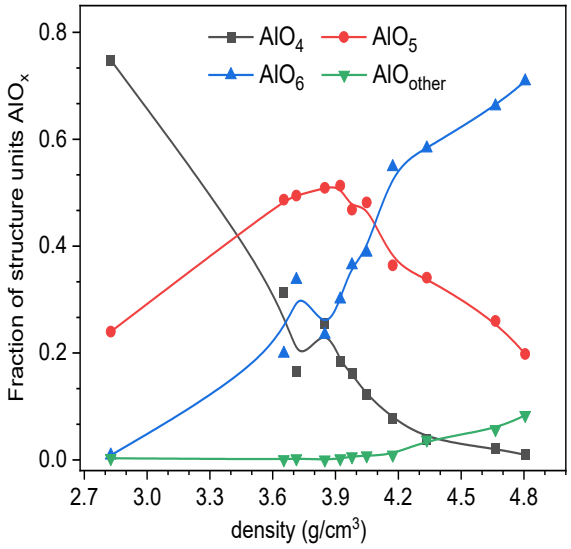


Figure 4. The dependence of fraction of $AlO_x$ unit on density in $Al_2O_3$ glass.

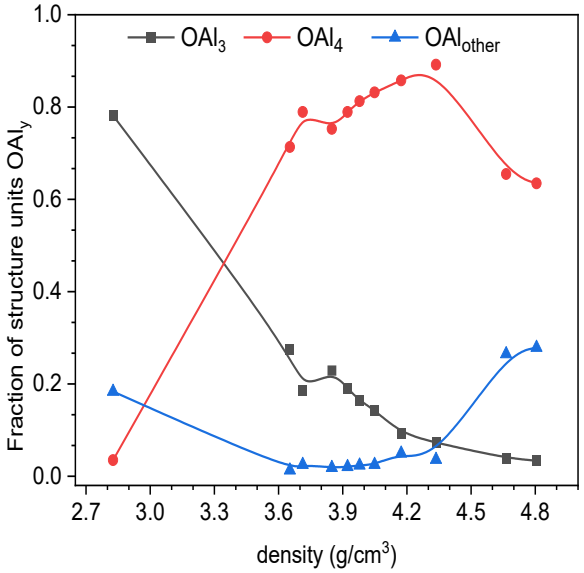


Figure 5. The dependence of fraction of $OAl_y$ units on density in $Al_2O_3$ glass.

We can see that the structure of $Al_2O_3$ is formed by $AlO_x$ structural units and their distribution is not uniform. They tend to form the clusters of $AlO_x$ units. The Fig. 6 presents the spatial distribution of structure unit AlOx (x=4,5,6) in Al2O3 model at different densities.

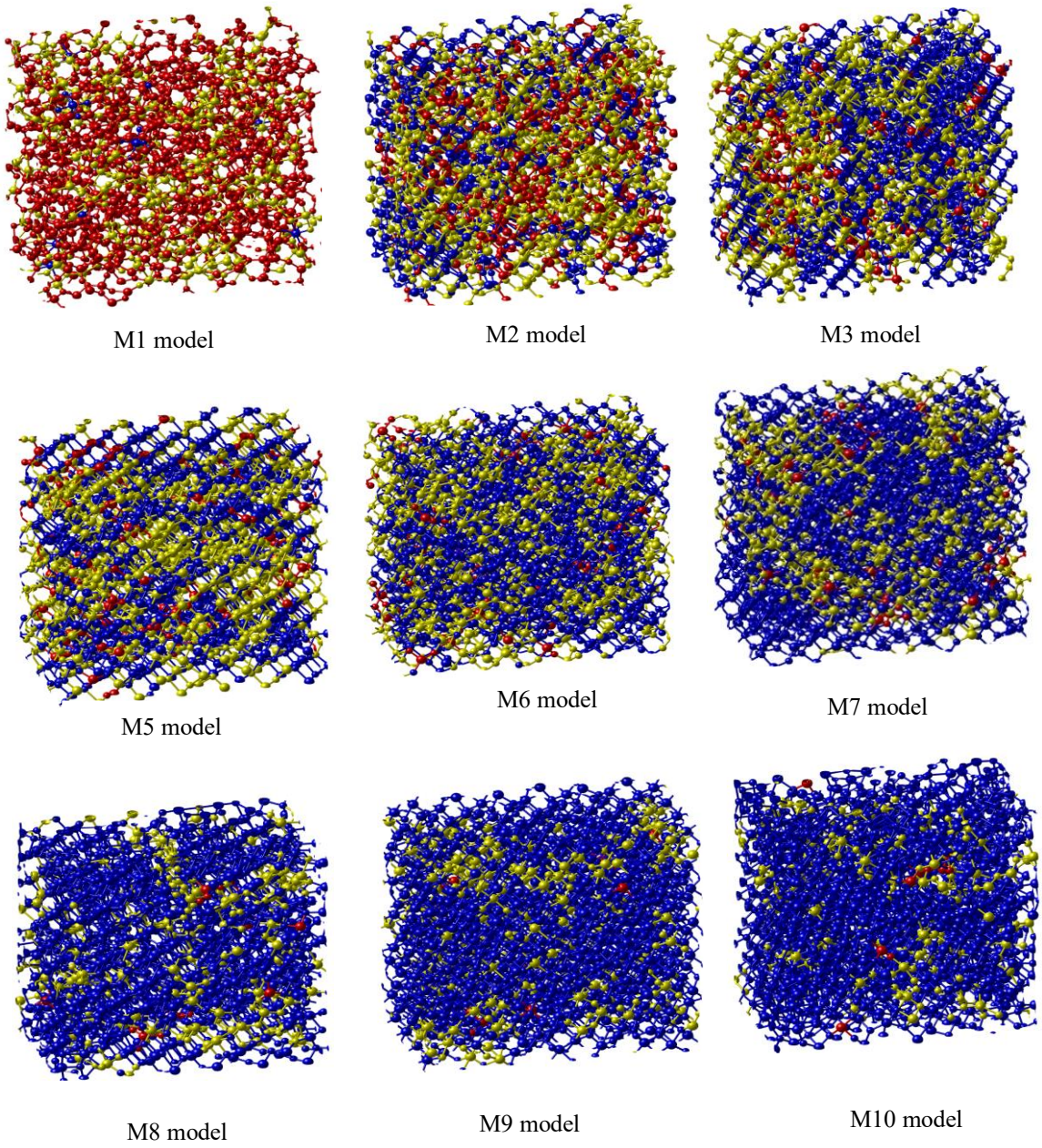


Figure 6. Spatial distribution of structure unit $AlO_x$ (x=4,5,6) in $Al_2O_3$ model at different densities. Here $AlO_4$, $AlO_5$, and $AlO_6$-clusters are illustrated by red, yellow, and blue, respectively.

The polymorphism and structural heterogeneity depend on the distribution of $AlO_x$ cluster. Therefore, we will calculate the size and spatial distribution of $AlO_x$ structural units to clarify the polymorphism and structural heterogeneity properties of $Al_2O_3$ glass. The detailed distributions of the number and sizes of $AlO_x$ clusters in $Al_2O_3$ glass melt at different densities are presented in Table 2. The results show that the $AlO_4$ coordination units form a large cluster of 4832 atoms meanwhile the $AlO_5$,

$AlO_6$- coordination units form several very small clusters at low density (2.83 g/cm$^3$). The largest $AlO_5$ cluster has 467 atoms. At the 3.71 g/cm$^3$ density, the structure of $Al_2O_3$ glass has a lot of small clusters of $AlO_4$ unit meanwhile the $AlO_5$ and $AlO_6$ units form a large cluster of 3913 atoms and 3329 atoms, respectively. In the range of density from 3.71 g/cm$^3$ to 4.34 g/cm$^3$ (intermediate density region), the $Al_2O_3$ structure exists two large cluster of $AlO_5$ and $AlO_6$ unit. At high density (4.81 g/cm$^3$), the $AlO_6$ coordination units also form a very large cluster with size of 4856 atoms. The $AlO_4$ coordination units form very small clusters meanwhile $AlO_4$ coordination units form cluster with size from 6 to 987 atoms. The simulation result is in good agreement with visualization results in Table 1 and Fig. 6.

Table 2. Size distribution of $AlO_4$-, $AlO_5$- and $AlO_6$- cluster at different densities. $N_c$ is the number of clusters; $N_a$ is the number of atoms per one cluster

| **M1** | | **M3** | | **M5** | | **M7** | | **M8** | | **M10** | |
|---|---|---|---|---|---|---|---|---|---|---|---|
| 2.83 g/cm$^3$ | | 3.71 g/cm$^3$ | | 3.92 g/cm$^3$ | | 4.17g/cm$^3$ | | 4.34 g/cm$^3$ | | 4.81 g/cm$^3$ | |
| $N_c$ | $N_a$ | $N_c$ | $N_a$ | $N_c$ | $N_a$ | $N_c$ | $N_a$ | $N_c$ | $N_a$ | $N_c$ | $N_a$ |
| 3 | 5 | 75 | 5 | 99 | 5 | 77 | 5 | 47 | 5 | 15 | 5 |
| 1 | 4832 | 27 | 9 | 33 | 9 | 18 | 9 | 6 | 9 | 1 | 13 |
| | | 1 | 12 | 9 | 13 | 1 | 12 | 1 | 24 | | |
| 48 | 6 | 6 | 13 | 1 | 16 | 4 | 13 | | | 44 | 6 |
| 12 | 10 | 1 | 16 | 5 | 17 | 1 | 16 | 24 | 6 | 1 | 9 |
| 7 | 11 | 9 | 17 | 2 | 21 | 2 | 17 | 2 | 11 | 1 | 10 |
| 2 | 14 | 1 | 20 | 1 | 24 | 2 | 21 | 1 | 16 | 4 | 11 |
| 3 | 15 | 2 | 21 | 1 | 29 | | | 1 | 2817 | 1 | 15 |
| 1 | 16 | 1 | 25 | 1 | 39 | 3 | 6 | | | 5 | 16 |
| 1 | 18 | 2 | 29 | 1 | 40 | 1 | 3090 | | | 1 | 18 |
| 2 | 19 | 1 | 33 | 1 | 53 | | | 1 | 4477 | 1 | 19 |
| 3 | 20 | 1 | 40 | 1 | 62 | | | | | 1 | 20 |
| 1 | 21 | 1 | 52 | 1 | 63 | 1 | 4322 | | | 1 | 21 |
| 1 | 22 | 1 | 102 | 1 | 77 | | | | | 1 | 25 |
| 4 | 23 | 1 | 162 | 1 | 121 | | | | | 1 | 26 |
| 3 | 24 | | | | | | | | | 1 | 30 |
| 2 | 26 | 1 | 11 | 1 | 6 | | | | | 1 | 35 |
| 1 | 27 | 1 | 3913 | 1 | 3999 | | | | | 1 | 54 |
| 1 | 33 | | | | | | | | | 1 | 103 |
| 1 | 37 | 6 | 7 | 8 | 7 | | | | | 1 | 108 |
| 1 | 42 | 1 | 18 | 1 | 3226 | | | | | 1 | 987 |
| 1 | 81 | 1 | 3329 | | | | | | | | |
| 1 | 82 | | | | | | | | | 1 | 4856 |
| 1 | 91 | | | | | | | | | | |
| 1 | 98 | | | | | | | | | | |
| 1 | 182 | | | | | | | | | | |
| 1 | 183 | | | | | | | | | | |
| 1 | 223 | | | | | | | | | | |
| 1 | 467 | | | | | | | | | | |
| 16 | 7 | | | | | | | | | | |
| 2 | 12 | | | | | | | | | | |

Investigation results reveal the local structural environment of Al and O is strongly dependent on density. The densification mechanism in aluminum system is due to the short-range order structure change of Al and O atoms. Therefore, to clarify the structural transformation mechanism under high density, the fractions of the Dx domain, the distributions of Core-, Edge and Face- sharing bond and the distribution of free volumes in $Al_2O_3$ glass are calculated. The Fig. 7 shows the dependence of domain atoms on the density in $Al_2O_3$ glass. It can be seen that the variation of the fraction of D4 domain and D6 domain in opposite directions. The curve for the fraction of D5 domain intersects with those of the D4 and D6 domains at 3.48g/cm and 4.05 g/cm$^3$ density, respectively. Thus, the $Al_2O_3$ structure exists only one phase (one domain) at low or high density and two phases (tow domains) at intermediate density region. These results consistent with fraction of coordination units in Fig 5. We existence of DB relates to the splitting and merging of domain. Changes in the fraction of DB atoms depend on the number of domains in model. The intensive splitting of D4 domains is the cause of the rapidly number of DB atoms. The merging of Dx domains intensively occurs at low or high density, meanwhile the splitting of domain intensively occurs within 3.65- 4.34 g/cm$^3$ density. As shown in Fig. 8, the fraction of oxygen in D4 domain monotonously decreases in opposite with the fraction of oxygen in D6 domains. This is caused by that the D4 and D6 domain have respectively large and small size at low density. In contrast at high density the size of D6 domain is larger than that of D4 domain. Therefore, the fraction of oxygen in Dx domains is correlated with size of domains. It means that the large size of Dx domain is cause of the growing of fraction of oxygen in Dx.

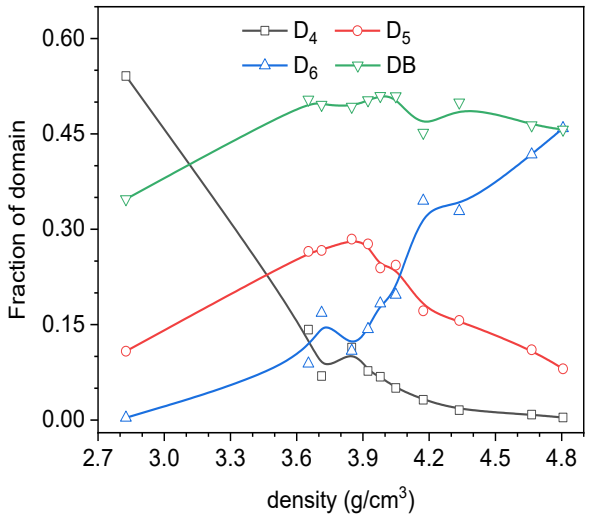


Figure 7. The dependence of domain atoms on the density in $Al_2O_3$ glass.

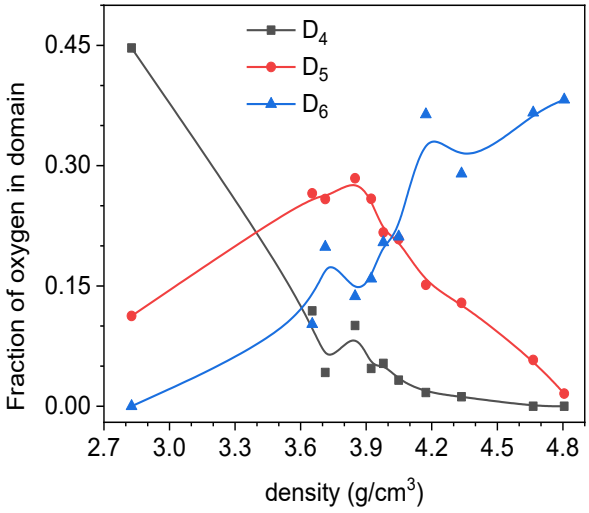


Figure 8. The dependence of oxygen in domain atoms on the pressure in $Al_2O_3$ glass.

These results can be seen from Table 3 showing the size distributions of domains at different densities. The number of domains having fewer atoms rapidly increases in range of density from 2.83 to 4.05 g/cm, and then it decreases at density larger than 4.05 g/cm$^3$. Moreover, almost all models contain one domain with size larger than 500 atoms (about 10% of total atoms). The detailed numbers and sizes of large Dx domains ($x=4,5,6$) is displayed in Table 4. The large domains Dx is the luster containing more than 30 atoms. The results reveal that at low density, model has only one large D4 domain with 2817 atoms. In intermediate density region, the model contains several large D5 and D6 domains. Under compression, the cluster domain D6 is bigger. There is one large D6 domain with 2145 atoms at 4.81 g/cm$^3$ (high density).

Table 3. The dependence of size distribution of domains on density

| Size range | Number domain | | | | | | | | | |
|---|---|---|---|---|---|---|---|---|---|---|
| | M1 | M2 | M3 | M4 | M5 | M6 | M7 | M8 | M9 | M10 |
| 1-4 atoms | 523 | 1235 | 1057 | 1115 | 1148 | 1106 | 879 | 928 | 667 | 558 |
| 5-19 atoms | 20 | 50 | 55 | 52 | 55 | 56 | 39 | 34 | 15 | 3 |
| 20-49 atoms | 0 | 12 | 8 | 6 | 7 | 16 | 5 | 4 | 0 | 0 |
| 50-99 atoms | 0 | 4 | 2 | 5 | 2 | 5 | 1 | 1 | 0 | 0 |
| 100-499 atoms | 0 | 1 | 1 | 3 | 2 | 0 | 0 | 0 | 0 | 0 |
| >500 atoms | 1 | 1 | 1 | 0 | 0 | 0 | 1 | 1 | 1 | 1 |

Our simulation shows that the $Al_2O_3$ glass has a number of large D4, D5 and D6 domains which have sizes bigger 5% of total atoms. It means that the domains having fewer atoms are uniformly distributed in the model, while the largest domain is spread over whole system. From Tables 3and 4, we can see that intermediate regions correspond to two-domain type and other regions (low-high density) are of one-domain type. The existence of two-domain type regions implies the polymorphism in glass.

Table 4. Number and size of large domains at different densities. Here $S_D$ is the size range for domains; $n_D$ is the number of domains.

| Model | M1 | | M3 | | M5 | | M7 | | M8 | | M10 | |
|---|---|---|---|---|---|---|---|---|---|---|---|---|
| | $S_D$ | $n_D$ | $S_D$ | $n_D$ | $S_D$ | $n_D$ | $S_D$ | $n_D$ | $S_D$ | $n_D$ | $S_D$ | $n_D$ |
| D4 | 2817 | 1 | - | - | - | - | - | - | - | - | - | - |
| D5 | - | - | 30 - 578 | 6 | 34-310 | 7 | 32- 40 | 3 | 35 | 1 | - | - |
| D6 | - | - | 30- 98 | 3 | 47 | 1 | 74-1424 | 2 | 55- 1265 | 2 | 2145 | 1 |

The structure of $Al_2O_3$ formed by a continuous random network of basic structural units. Two $AlO_x$ units are linked to each other by a common oxygen atom, which is called “bridge oxygen”. The connectivity can involve one, two, or three bridging oxygens (BOs). They are called corner-sharing, edge-sharing, face-sharing bond, respectively.

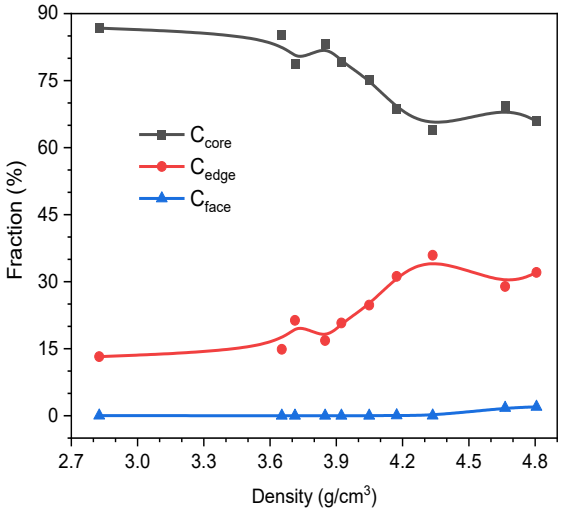


Figure 9. The dependence of fraction of different bridge-oxygen connectivity on density.

To investigate the influence of density on short-range order, linking of basic structural unit, we calculated distribution of the number of corner-, edge- and face-sharing bonds as well as their length

Table 5. The distribution of Core-, Edge and Face- sharing bond at different pressures in $Al_2O_3$ glass. $N_{core}$, $N_{edge}$, $N_{face}$ is the number of core-, edge and cace- sharing bond, respectively

| Density(g/cm$^3$) | $N_{core}$ | $N_{edge}$ | $N_{face}$ |
|---|---|---|---|
| 2.83 | 6855 | 1046 | 2 |
| 3.65 | 9660 | 1687 | 0 |
| 3.71 | 9586 | 2601 | 0 |
| 3.85 | 9689 | 1959 | 0 |
| 3.92 | 9524 | 2496 | 1 |
| 4.05 | 9345 | 3075 | 0 |
| 4.17 | 8755 | 3972 | 9 |
| 4.34 | 8253 | 4629 | 5 |
| 4.66 | 9795 | 4087 | 247 |
| 4.81 | 9449 | 4593 | 285 |

According to results of Table 5, the $AlO_x$ basic structural unit mainly link to each other via corner, edge- sharing bonds. There is only the small number of face-sharing bond at high density. The fractions of corner-, edge- and face-sharing bonds also changed gradually with density and can be seen Fig 9. Namely, at low density (2.83 g/cm$^3$), the basic structural units are mainly linked via bridge oxygen (BO) and the connectivity between $AlO_x$ is mainly corner sharing bonds (86.74%). The variations of corner sharing bonds and edge sharing bonds in opposite directions. Under compression, the number corner sharing bonds decreases and edge sharing bonds increases. The fraction of edge sharing bonds is equal to 13.24% at 2.83 g/cm$^3$ and it increases to 32.06% at 4.81 g/cm$^3$(high density).

Table 6. The distribution of average corner-, edge-, face-sharing bond length at different pressures in $Al_2O_3$ glass. $D_c$, $D_e$ and $D_f$ are the average-distance of corner-sharing bonds, edge-sharing bonds and face-sharing bonds, respectively

| Density(g/cm$^3$) | $D_c$ (Å) | $D_e$ (Å) | $D_f$ (Å) |
|---|---|---|---|
| 2.83 | 3.173 | 2.787 | - |
| 3.65 | 3.168 | 2.991 | - |
| 3.71 | 3.113 | 2.963 | - |
| 3.85 | 3.143 | 2.973 | - |
| 3.92 | 3.138 | 2.971 | - |
| 4.05 | 3.131 | 2.950 | - |
| 4.17 | 3.138 | 2.921 | - |
| 4.34 | 3.130 | 2.907 | - |
| 4.66 | 3.136 | 2.824 | - |
| 4.81 | 3.132 | 2.804 | - |

Table 6 shows the distributions of average corner-, edge-, face-sharing bond lengths at different densities. We can be seen that the average corner sharing bond lengths is about 3.173 Å at low density and it is almost not dependent on the density. Meanwhile, the result also shows the increase of the average edge-sharing bond lengths with compression. At low density (2.83 g/cm$^3$), the average lengths of edge-sharing bonds are around 2.787 Å. However, the increase of the average edge-sharing bond

lengths is small. At the high density (4.81 g/cm$^3$), it is equal to 2.804 Å. The number of face-sharing bonds is too small to calculate the average length.

There are many free volume regions (where no atoms can occupy) in material. The free volume has the effect on structure as well as mechanical-, physical- and chemical-properties. Therefore, we investigated the effect of density on free volume regions. In which, the free volume regions were calculated via a sphere passing four neighboring atoms without atom inside. The radius of sphere is not fixed, it depends only on position of four neighboring atoms. The radius distribution of void is given in Fig. 10.

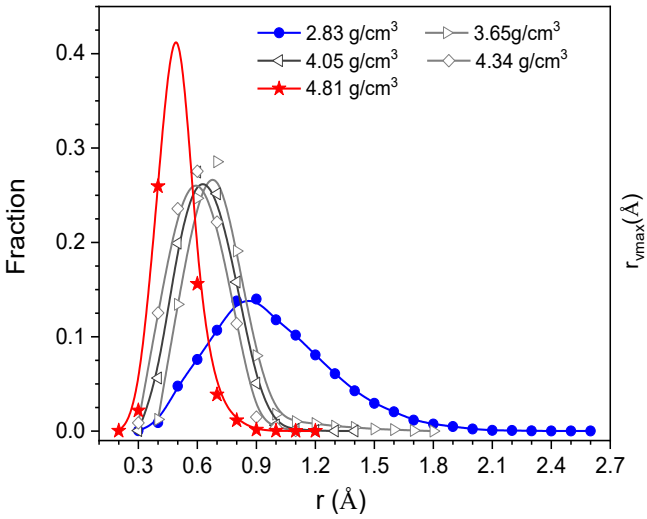


Figure 10. The radius distribution of void in $Al_2O_3$ glass under densification

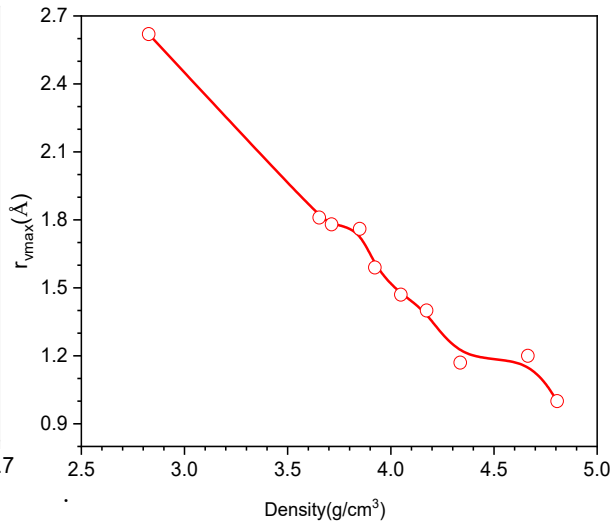


Figure 11. The dependence of the radius of largest void on density in $Al_2O_3$ glass.

The distribution of void radii exhibits a Gaussian form. There is a pronounced peak and its position tends to shifts to the left under compression. The shape of distribution of void radius strongly changes with density. The lower density, the lower the height of the distribution of void radius peak. And the curve is broader. Namely, the position of the peak of fraction of void radius is from 0.9Å to 0.6Å and the height of the distribution of void radius reduced from 0.44 to 0.14 in range of density from 2.83 to 4.81 g/cm$^3$. Moreover, the void radii decrease rapidly under densification. At low density (2.83 g/cm$^3$), the radius of largest void ($r_{vmax}$) is 2.6 Å whereas it decreases to 1.2 Å at high density (4.81 g/cm$^3$). The dependence of the radius of largest void on density is displayed in Fig. 11.

## 4. Conclusion

We have investigated structure of alumina glass at 600 K under different densities by MD simulation. The simulation reveals that the $Al_2O_3$ structure exists only one phase (one domain) at low or high density and two phases (tow domains) at intermediate density region. The $AlO_x$ structural units tend to form clusters and their distribution is not uniform. Under densification, the bond Al-O bond distance is almost not changing meanwhile the Al-Al and O-O bond distance is significantly change. The Al-O bond distance is equal to 1.70±0.02 Å. The basic structural units link to each other via with corner-sharing, edge-sharing, face-sharing bonds. At low density region, the basic structural units are

mainly linked via corner sharing bonds. The average corner- sharing bond lengths is about 3.173 Å at low density and it is almost not dependent on the density. In the $Al_2O_3$, the basic structural units are barely bonded to each other via face-sharing bond. Moreover, the distribution of free volumes has the Gaussian form and the shape of distribution of void radius strongly changes with density. The position of the peak tends to shift to the left under compression. The lower density, the lower the height of the distribution of void radius peak. The position of the peak of fraction of void radius is from 0.9Å to 0.6Å and the height of the distribution of void radius reduced from 0.44 to 0.14 in range of density from 2.83 to 4.81 g/cm$^3$. As density increases, the void radius decreases rapidly.

## References


[1] M. I. Ojovan, Viscosity and Glass Transition in Amorphous Oxides, Advances in Condensed Matter Physics, Vol. 2008, 2008, pp. 817829, https://doi.org/10.1155/2008/817829.

[2] Y. Zhao, X. Bian, X. Hou, Viscosity and Fragility of the Supercooled and Superheated Liquids of the $Ni_{60}Zr_{30}Al_{10}$ Metallic Glass-forming Alloy, Physica A: Statistical Mechanics and its Applications, Vol. 367(C), 2006, pp. 42-54, https://doi.org/10.1016/j.physa.2005.11.020.

[3] K. S. Shamala, L. C. S. Murthy, M. C. Radhakrishna, K. N. Rao, Characterization of $Al_2O_3$ thin Films Prepared by Spray Pyrolysis Method for Humidity Sensor, Sensors and Actuators A: Physical, Vol. 135, No. 2, 2007, pp. 552-557, https://doi.org/10.1016/j.sna.2006.10.004.

[4] J. H. Park, T. Suzuki, M. Kurosawa, M. Miyao, T. Sadoh, Nucleation-Controlled Gold-Induced-Crystallization for Selective Formation of Ge(100) and (111) on Insulator at Low-Temperature (~250 °C), Applied Physics Letters, Vol. 103, No. 8, 2013, pp. 082102, https://doi.org/10.1063/1.4819015.

[5] Y. N. Novikov, V. A. Gritsenko, K. A. Nasyrov, Charge Transport Mechanism in Amorphous Alumina, Applied Physics Letters, Vol. 94, No. 22, 2009, pp. 222904, https://doi.org/10.1063/1.3151861.

[6] I. Jackson, Melting of the Silica Isotopes $SiO_2$, $BeF_2$ and $GeO_2$ at Elevated Pressures, Physics of the Earth and Planetary Interiors, Vol. 13, No. 3, 1976, pp. 218–231, https://doi.org/10.1016/0031-9201(76)90096-0.

[7] P. S. Salmon, A. Zeidler, Networks under Pressure: the Development of in Situ High-Pressure Neutron Diffraction for Glassy and Liquid Materials, Journal of Physics: Condensed Matter, Vol. 27, No. 13, 2015, pp. 133201, https://doi.org/10.1088/0953-8984/27/13/133201.

[8] Q. Mei, S. Sinogeikin, G. Shen, S. Amin, C. J. Benmore, K. Ding, High-pressure X-ray Diffraction Measurements on Vitreous $GeO_2$ under Hydrostatic Conditions, Physical Review B, Vol. 81, No. 17, 2010, pp. 174113, https://doi.org/10.1103/PhysRevB.81.174113.

[9] J. W. E. Drewitt, P. S. Salmon, A. C. Barnes, S. Klotz, H. E. Fischer, W. A. Crichton, Structure of $GeO_2$ Glass at Pressures up to 8.6 GPa, Physical Review B, Vol. 81, No. 1, 2010, pp. 014202, https://doi.org/10.1103/PhysRevB.81.014202.

[10] G. Lelong, L. Cormier, G. Ferlat, V. Giordano, G. S. Henderson, A. Shukla, G. Calas, Evidence of Fivefold-coordinated Ge Atoms in Amorphous $GeO_2$ under Pressure, Physical Review B, Vol. 85, No. 13, 2012, pp. 134202, https://doi.org/10.1103/PhysRevB.85.134202.

[11] C. Shi, O. L. G. Alderman, D. Berman, J. Du, J. Neuefeind, A. Tamalonis, J. K. R. Weber, J. You, C. J. Benmore, The Structure of Amorphous and Deeply Supercooled Liquid Alumina, Frontiers in Materials, Vol. 6, 2019, pp. 38, https://doi.org/10.3389/fmats.2019.00038.

[12] A. F. Harper, K. Iwanowski, W. C. Witt, M. C. Payne, M. Simoncelli, Vibrational and Thermal Properties of Amorphous Alumina from First Principles, Physical Review Materials, Vol. 8, No. 4, 2024, pp. 043601, https://doi.org/10.1103/PhysRevMaterials.8.043601.

[13] W. Li, Y. Ando, S. Watanabe, Effects of Density and Composition on the Properties of Amorphous Alumina: A High-Dimensional Neural Network Potential Study, the Journal of Chemical Physics, Vol. 153, No. 16, 2020, pp. 164119, https://doi.org/10.1063/5.0026289.

[14] Florian, D. Massiot, B. Poe, I. Farnan, J. P. Coutures, A Time Resolved $^{27}$Al NMR Study of the Cooling Process of Liquid Alumina from 2450 °C to Crystallisation, Solid State Nuclear Magnetic Resonance, Vol. 5, No. 4, 1995, pp. 233-238, https://doi.org/10.1016/0926-2040(95)01188-X.

[15] D. R. Neuville, D. de Ligny, L. Cormier, G. S. Henderson, J. Roux, A. Flank, The Crystal and Melt Structure of Spinel and Alumina at High Temperature: an In-situ XANES Study at the Al and Mg K-edges, Geochimica et Cosmochimica Acta, Vol. 73, No. 11, 2009, pp. 3410-3422, https://doi.org/10.1016/j.gca.2009.02.033.

[16] S. K. Lee, S. Ryu, Probing of Triply Coordinated Oxygen in Amorphous $Al_2O_3$, The Journal of Physical Chemistry Letters, Vol. 9, No. 1, 2018, pp. 150-156, https://doi.org/10.1021/acs.jpclett.7b03027.

[17] F. Harper, S. P. Emge, P. C. M. M. Magusin, C. P. Grey, A. J. Morris, Modelling Amorphous Materials Via a Joint Solid-state NMR and X-ray Absorption Spectroscopy and DFT Approach: Application to Alumina, Chemical Science, Vol. 14, No. 5, 2023, pp. 1155-1167, https://doi.org/10.1039/D2SC04035B.

[18] P. Lamparter, R. Kniep, Structure of Amorphous $Al_2O_3$, Physica B: Condensed Matter, Vol. 234-236, 1997, pp. 405-406, https://doi.org/10.1016/S0921-4526(96)01044-7.

[19] H. Hashimoto, Y. Onodera, S. Tahara, S. Kohara, K. Yazawa, H. Segawa, M. Murakami, K. Ohara, Structure of Alumina Glass, Scientific Reports, Vol. 12, 2022, pp. 516, https://doi.org/10.1038/s41598-021-04455-6.

[20] M. Hemmati, M. Wilson, P. A. Madden, Structure of Liquid $Al_2O_3$ from a Computer Simulation Model, The Journal of Physical Chemistry B, Vol. 103, No. 20, 1999, pp. 4023-4028, https://doi.org/10.1021/jp983529f.

[21] D. J. Lacks, First-Order Amorphous-Amorphous Transformation in Silica, Physical Review Letters, Vol. 84, No. 20, 2000, pp. 4629-4632, https://doi.org/10.1103/PhysRevLett.84.4629.

[22] V. V. Hoang, Structure and Dynamics of Liquid and Amorphous $Al_2O_3 \cdot 2SiO_2$, The European Physical Journal Applied Physics, Vol. 33, No. 1, 2006, pp. 69-76, https://doi.org/10.1051/epjap:2006137.

[23] L. B. Skinner, A. C. Barnes, P. S. Salmon, L. Hennet, H. E. Fischer, C. J. Benmore et al., Joint Diffraction and Modeling Approach to the Structure of Liquid Alumina, Physical Review B, Vol. 87, No. 2, 2013, pp. 024201, https://doi.org/10.1103/PhysRevB.87.024201.

[24] V. V. Hoang, About an Order of Liquid–liquid Phase Transition in Simulated Liquid $Al_2O_3$, Physics Letters A, Vol. 335, No. 5-6, 2005, pp. 439-443, https://doi.org/10.1016/j.physleta.2004.12.040.

[25] V. V. Hoang, S. K. Oh, Simulation of Pressure-induced Structural Transformation in Liquid and Amorphous $Al_2O_3$, Physical Review B, Vol. 72, No. 5, 2005, pp. 054209, https://doi.org/10.1103/PhysRevB.72.054209.

[26] P. K. Hung, T. Vinh, Local Microstructure of Liquid and Amorphous $Al_2O_3$, Journal of Non-Crystalline Solids, Vol. 352, No. 52-54, 2006, pp. 5531-5540, https://doi.org/10.1016/j.jnoncrysol.2006.09.016.

[27] G. Gutierrez, B. Johansson, Molecular Dynamics Study of Structural Properties of Amorphous $Al_2O_3$, Physical Review B, Vol. 65, No. 10, 2002, pp. 104202, https://doi.org/10.1103/PhysRevB.65.104202.

[28] X. Zhou, Y. Zhou, Y. Deng, Y. Zhang, Structural, Vibrational and Transport Properties of Liquid and Amorphous Alumina: A Molecular Dynamics Simulation Study, Frontiers in Materials, Vol. 9, 2022, pp. 1005747, https://doi.org/10.3389/fmats.2022.1005747.